
**DESCRIPTION OF HADRON INELASTIC SCATTERING
BY THE LAPLACE METHOD AND NEW MECHANISMS
OF CROSS-SECTION GROWTH**

**I.V. SHARF, A.V. TYKHONOV, G.O. SOKHRANNYI, K.V. YATKIN,
M.A. DELIYERGIYEV, N.A. PODOLYAN, V.D. RUSOV**

PACS 13.85.-t, 13.85.Lg
©2011

Odesa National Polytechnical University
(1, Shevchenko Prosp., Odesa 650044, Ukraine)

It is shown that there exist some types of Feynman diagrams, which can be calculated within the Laplace method. This allows one to reveal new mechanism of growth of the scattering cross-sections, which are not involved by the Regge theory due to the neglect of the dependence of the scattering amplitude on the longitudinal components of the momenta of secondary particles in the center-of-mass system of initial state particles. Within the multiperipheral model, the energy dependence of the total scattering cross-section is obtained. The theoretical results coincide qualitatively with experimental data.

1. Introduction

In the analysis of the hadron-hadron scattering at high energies, the main attention is paid to the elastic scattering. It is considered that the problem of describing the elastic scattering is much simpler, compared with the description of inelastic processes. Therefore, one may try to calculate firstly the elastic scattering amplitude and then to determine the contributions of various inelastic processes from its imaginary part [1, 2].

However, the direct consideration of inelastic processes seems more expedient, in our opinion. First, such processes present a greater information about the properties of colliding particles. Indeed, the parameters that remain hidden in characteristics of virtual particles in the elastic processes can be determined in terms of characteristics of real particles, which are directly observed, in the inelastic processes. In addition, since the elastic scattering amplitude contains the information about all processes realized at the scattering due to the unitarity

condition, the “proper” elastic scattering amplitude can hardly be a sufficiently simple function of its arguments.

But this reasoning has a meaning only if there exists a sufficiently efficient method to describe the inelastic processes. Namely the discussion of such a method is the purpose of the present work.

Typical process of inelastic scattering at relativistic energies consists in the collision of two bunches of particles with four-momenta P_1 and P_2 , respectively and as result we got n of secondary particles with four-momenta p_1, p_2, \dots, p_n and initial particles with changed four-momenta P_3 and P_4 . The general diagram of this process is given in Fig. 1, and its cross-section is given by the relation

$$\sigma_n = \frac{(2\pi)^4}{4n!I} \int \frac{d\mathbf{P}_3}{2P_{30} (2\pi)^3} \frac{d\mathbf{P}_4}{2P_{40} (2\pi)^3} \prod_{k=1}^n \frac{d\mathbf{p}_k}{2p_{0k} (2\pi)^3} \times$$

$$\times |T(n, \mathbf{p}_1, \mathbf{p}_2, \dots, \mathbf{p}_n, \mathbf{P}_1, \mathbf{P}_2, \mathbf{P}_3, \mathbf{P}_4)|^2 \times$$

$$\times \delta \left(P_3 + P_4 + \sum_{k=1}^n p_k - P_1 - P_2 \right), \quad (1)$$

where M_1 and M_2 are the masses of primary colliding particles; P_1 and P_2 are their four-momenta; and $I = \sqrt{(P_1 P_2)^2 - (M_1 M_2)^2}$ is the invariant flux.

It is accepted that the particles with four-momenta P_3 and P_4 are of the same sorts as those with four-momenta P_1 and P_2 , and n secondary particles with four-momenta p_1, p_2, \dots, p_n are identical. By $T(n, \mathbf{p}_1, \mathbf{p}_2, \dots, \mathbf{p}_n, \mathbf{P}_1, \mathbf{P}_2, \mathbf{P}_3, \mathbf{P}_4)$, we denote the scattering amplitude corresponding to the inelastic process

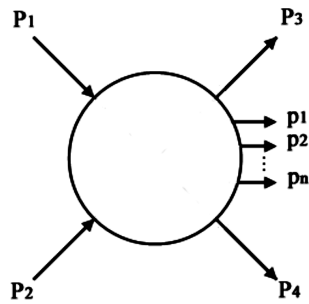


Fig. 1. General diagram of inelastic scattering

in Fig. 1, and δ stands for the four-dimensional Dirac δ -function ensuring the laws of conservation of energy and three components of the momentum.

The calculation of the multidimensional integral (1) is a complicated task. However, it can be simplified in the case where the modulus of the scattering amplitude has a constrained maximum point on the condition that imposes on the arguments of the amplitude the presence of δ -function in the integrand of (1) and under the mass-shell conditions for all real particles. Then the integral can be calculated by the well-known Laplace method [3]. Representing the squared modulus of the scattering amplitude in (1) in the form $|T|^2 = \exp(\ln(|T|^2))$, we can expand the exponent in the Taylor series in a neighborhood of constrained maximum point, by restricting ourselves by quadratic terms. After that we obtain Gaussian integral, whose calculation is reduced to computation of matrix determinant of the second derivatives of $\ln(|T|^2)$.

Here, we consider several types of Feynman diagrams corresponding to the scattering amplitudes which allow us to make calculation by the Laplace method. The application of this method to the multiperipheral model allowed one to find new mechanisms of cross-sections growth [4, 5] and to reconstruct the dependence of the energy dependence of the total cross-section which coincides qualitatively with experimental data. At the same time, the use of the Laplace method allows us to go out of the boundaries of the multiperipheral model and to analyze some types of nonmultiperipheral diagrams of inelastic scattering, which will be considered in what follows.

Intending to develop firstly a model simplest for the analysis, we will consider the primary and secondary hadrons, as well as the virtual particles, as quanta of the effective scalar interacting and self-interacting fields. We can also consider the diagrams of a more realistic theory, namely the quantum chromodynamics (QCD). As will be shown below, these diagrams in the diagonal gauge contain the same factors as those in the simplest scalar

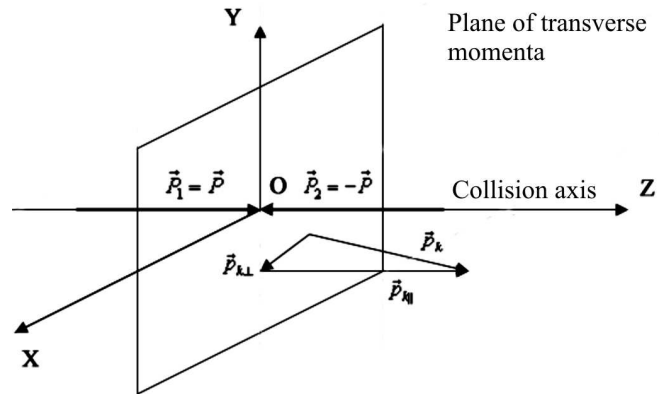


Fig. 2. Decomposition of the three-dimensional momenta of secondary particles into longitudinal and transverse components relative to the collision axis in the center-of-mass system of input particles with three-dimensional momenta P_1 and P_2

theory. Therefore, all main results concerning the existence of the maximum point, its properties, and mechanisms determining the behavior of cross-sections can be transferred onto the QCD diagrams.

In addition, in order to simplify the problem, we will consider the collision of primary particles with the same mass, i.e., $M_1 = M_2 = M$. In the numerical calculations, we took M equal to the proton mass and m equal to 0.139 GeV, which is approximately equal to the pion mass. While performing the numerical and analytic calculations, all quantities were made dimensionless in units of the mass of a secondary particle m . Therefore, we set $m = 1$ in all subsequent calculations.

Thus, the goal of this report is to prove the possibility of applying the Laplace method for some types of Feynman diagrams, and demonstrate the possibilities of the method for calculating these diagrams.

2. Extraction of Independent Parameters of the Scattering Amplitude

Since the scattering cross-section is a Lorentz-invariant quantity, it can be calculated in any inertial frame of reference. The most convenient for the calculations is the center-of-mass system of initial particles, where the momenta of these particles are equal in modulus and are opposite in directions, as is shown in Fig. 2.

In this reference system, we have the collision axis (Fig. 2), along which the momenta of initial particles are directed. It is convenient to decompose all three-dimensional momenta into the following components: parallel to the axis, $p_{k\parallel}$, and perpendicular to it, $\vec{p}_{k\perp}$ (i.e., the component in the plane of transverse mo-

menta in Fig. 2). As usual, we denote the total energy of primary particles in their center-of-mass system by \sqrt{s} and choose the coordinate axes so as it is shown in Fig. 2.

The equations representing the law of conservation of energy-momentum are those of connection between arguments of the scattering amplitude. Our purpose is to express some four variables from this system of equations in terms of the remaining $3n + 2$ independent variables. To this end, it is convenient to introduce the new variables

$$P_{\parallel}^s = \frac{P_{3\parallel} + P_{4\parallel}}{2}, \quad P_{\parallel}^a = \frac{P_{3\parallel} - P_{4\parallel}}{2},$$

$$P_{\perp x}^s = \frac{P_{3\perp x} + P_{4\perp x}}{2}, \quad P_{\perp x}^a = \frac{P_{3\perp x} - P_{4\perp x}}{2},$$

$$P_{\perp y}^s = \frac{P_{3\perp y} + P_{4\perp y}}{2}, \quad P_{\perp y}^a = \frac{P_{3\perp y} - P_{4\perp y}}{2}. \quad (2)$$

In addition, it is convenient to introduce the rapidities y_k instead of the components of the momentum, p_{kz} , which are parallel to the collision axis, with the help of the relation

$$p_{kz} = m_{\perp}(\mathbf{p}_{k\perp}) \operatorname{sh}(y_k), \quad (3)$$

where $m_{\perp}(\mathbf{p}_{k\perp}) = \sqrt{1 + (p_{k\perp x})^2 + (p_{k\perp y})^2}$.

Then we choose the following $3n + 2$ independent variables: n rapidities of secondary particles y_1, y_2, \dots, y_n , n components of the transverse momenta of secondary particles along the axis x ($p_{k\perp x}, k = 1, 2, \dots, n$), n analogous components along the axis y ($p_{k\perp y}, k = 1, 2, \dots, n$), and $P_{\perp x}^a$ and $P_{\perp y}^a$.

The variables P_{\parallel}^s , $P_{\perp x}^s$, and $P_{\perp y}^s$ can be easily represented in terms of the chosen independent variables from the laws of conservation of components of the momentum. Then the energy conservation law can be considered as an equation for P_{\parallel}^a . It has two solutions:

$$P_{\parallel}^a = \frac{f_1 P_{P\parallel} \pm \frac{E_P}{2} \sqrt{(f_1)^2 + f_2(f_2 - f_3)}}{f_2},$$

$$f_1 = P_x P_{\perp x}^a + P_y P_{\perp y}^a, \quad f_2 = \frac{(E_P)^2}{4} - (P_{P\parallel})^2,$$

$$f_3 = M^2 + (P_x)^2 + (P_y)^2 + (P_{\perp x}^a)^2 + (P_{\perp y}^a)^2, \quad (4)$$

where we introduced the following designations:

$$E_P = \sqrt{s} - \sum_{k=1}^n m_{\perp}(\mathbf{p}_{k\perp}) \operatorname{ch}(y_k),$$

$$P_x = -\frac{1}{2} \sum_{k=1}^n p_{k\perp x}, \quad P_y = -\frac{1}{2} \sum_{k=1}^n p_{k\perp y},$$

$$P_{P\parallel} = -\frac{1}{2} \sum_{k=1}^n m_{\perp}(\mathbf{p}_{k\perp}) \operatorname{sh}(y_k). \quad (5)$$

It is clear from the symmetry of the problem that if the modulus of the scattering amplitude has a maximum, it should be attained in the center-of-mass system at zero transverse momenta of all particles. Indeed, if the maximum would be attained at a nonzero value of the transverse momentum vector of any particle, then this vector would separate some direction in the plane of transverse momenta. But all directions in this plane (Fig. 2) are physically equivalent.

It is seen from expressions (4) that, at zero transverse momenta, the sign of the quantity P_{\parallel}^a coincides with the chosen sign of the root in (4). We note that, on the diagram in Fig. 1, the particle with momentum \mathbf{P}_3 is formed from the input particle with \mathbf{P}_1 with a positive value of the longitudinal momentum, whereas the particle with momentum \mathbf{P}_4 is formed from the input particle with \mathbf{P}_2 with a negative value of the longitudinal momentum. Therefore, we may conclude that the most probable is the configuration of momenta, where $P_{3\parallel} > 0$ and $P_{4\parallel} < 0$. It follows from (2) that $P_{\parallel}^a > 0$ for the most probable configuration of momenta. For this reason, we choose the sign "plus" in (4) hereafter.

Thus, the law of conservations of energy-momentum results in the following relations between the variables:

$$P_{3\parallel} = P_{\parallel}^a + P_{\parallel}^s,$$

$$P_{\perp x}^s = -\frac{1}{2} \sum_{k=1}^n p_{k\perp x}, \quad P_{\perp y}^s = -\frac{1}{2} \sum_{k=1}^n p_{k\perp y}, \quad (6)$$

where $P_{\parallel}^s = -(1/2) \sum_{k=1}^n m_{\perp}(\mathbf{p}_{k\perp}) \operatorname{sh}(y_k)$, which follows from the law of conservation of the longitudinal component of the momentum.

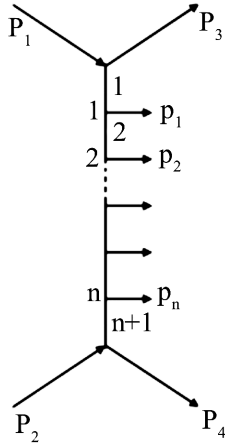


Fig. 3. Typical diagram of the multiperipheral model (numbers on the left and on the right are the numbers of vertices of the diagram and virtual lines, respectively)

3. Laplace Method for Diagrams of the Multiperipheral Model

The multiperipheral model [6] has been considered in high-energy physics for a very long time. But the application of the Laplace method to the calculation of scattering cross-sections in this model allows one to reveal its new specific features, which can turn out useful for the description of experimental data. A typical diagram of this model is shown in Fig. 3.

Such diagrams appear in a model, where the primary and secondary particles are considered as quanta of two interacting real scalar fields: $\Phi(x)$ with mass M (its quanta are considered as a model of primary particles) and $\varphi(x)$ with mass m . The Lagrangian of the model takes the form

$$\tilde{L} = \frac{1}{2} (g^{ab} \Phi_{,a} \Phi_{,b} - M^2 \Phi^2) + \frac{1}{2} (g^{ab} \varphi_{,a} \varphi_{,b} - m^2 \varphi^2) + g \Phi^2 \varphi + \lambda \varphi^3, \quad (7)$$

where g^{ab} are components of the Minkowski tensor, and g and λ are the coupling constants.

The partial cross-section (1) can be represented in the form [5]

$$\sigma_n(\sqrt{s}) = \frac{(2\pi)^2 g^4}{16m^2} \left(\frac{\lambda^2}{2(2\pi)^3} \right)^n \sigma'_n(\sqrt{s}), \quad (8)$$

where the function $\sigma'_n(\sqrt{s})$ free from insignificant constants determines the dependence of the cross-section on the energy \sqrt{s} .

The scattering amplitude corresponding to the diagram Fig. 3, up to an unessential constant factor for the maximization problem (which distinguishing the quantity A of the considered above quantity T), has the form

$$A = \prod_{l=1}^{n+1} (1 - (k_l)^2 - i\varepsilon)^{-1}, \quad (9)$$

where $k_1 = P_1 - P_3$, $k_2 = P_1 - P_3 - p_1, \dots, k_{n+1} = P_1 - P_3 - \sum_{j=1}^n p_j$. Here, $(k_l)^2$ means the scalar squares of relevant four-vectors in the Minkowski space, and the quantity ε responsible for the proper bypass of poles must be turned to zero after the execution of all calculations. In addition, we assume that the appropriate components of the four-vector P_3 are expressed in terms of independent variables by relations (6). We recall that all quantities are made dimensionless with the mass of a secondary particle m .

It is possible to prove that all quantities $(k_l)^2$ (they are called virtualities in what follows) are negative in the physical region of the process under consideration (the detailed proof is given in [4]). Therefore, amplitude (7) contains no poles in the region, over which we intend to integrate (1). This allows us to turn ε values to zero prior to the start of subsequent calculations. Then, as is seen from (9), the scattering amplitude takes only real positive values. Therefore, instead of the further study of function (9) for the maximum of its squared modulus, we can study the very function for the maximum.

It follows from (3), (4), and (9) that since $\mathbf{P}_{1\perp} = 0$ in the center-of mass system, all transverse components of momenta appear in the scattering amplitude only in the form of quadratic and bilinear combinations. This implies that, at zero values of all transverse components of momenta, we have at least a stationary point of the scattering amplitude. But if we take the symmetry-based reasoning presented in the previous section into account, then the subsequent search for the maximum can be carried on not for amplitude (9) itself, but for its restriction, which can be obtained, by setting all transverse components of momenta to be zero in (3)–(6) and (9). This restriction, which remains a function of only the number of secondary particles and their rapidities, is denoted as $A_{\parallel}(n, y_1, y_2, \dots, y_n)$.

Let us consider that the diagrams of the multiperipheral model have the horizontal axis of symmetry (Fig. 4).

It was shown in [4] that the quantity $A_{\parallel}(n, y_1, y_2, \dots, y_n)$ remains invariant under the simultaneous replacements of y_1 by $(-y_n)$, y_2 by $(-y_{n-1})$, etc., i.e., under the change of the rapidity of

each particle by the rapidity of the particle symmetric relative to the symmetry axis with the opposite sign. This follows from the symmetry of the process under the mirror reflection relative to the plane of transverse momenta (see Fig. 2). This symmetry implies that, at the maximum point, the rapidities of particles, which are joined to the diagram symmetrically relative to the symmetry axis (see Fig. 4), must take mutually opposite values; if the number of particles is odd, the rapidity of the particle, which belongs to the symmetry axis (Fig. 4, *b*), must be equal to zero [4]. Thus, by setting the rapidities in the lower part of the diagram in Fig. 4 to be equal to the corresponding rapidities of particles of the upper part taken with the sign “minus” and the rapidity of the particle that belongs to the symmetry axis to be zero, we obtain the further restriction of the scattering amplitude, which is a function of only the rapidities of particles placed above the symmetry axis (Fig. 4). We denote it by A_0 .

In the case where the number of particles is even, we have [4]

$$A_0 = \left(\prod_{j=1}^{n/2} \left(1 - (E_j)^2 + (P_{\parallel j})^2 \right)^{-2} \right) \times \left(1 + (P_{\parallel n/2+1})^2 \right)^{-1}. \quad (10)$$

Here, the energy transferred along the line with the number j (Fig. 3) is

$$E_j = \sum_{k=j}^{n/2} \text{ch}(y_k), \quad (11)$$

if $j = 1, 2, \dots, n/2$, and $E_{n/2} = 0$, and the longitudinal component of the momentum

$$P_{\parallel j} = P_{1\parallel} - P_{3\parallel} - \sum_{k=1}^{j-1} \text{sh}(y_k), \quad (12)$$

for $j = 2, 3, \dots, n/2 + 1$, and $P_{\parallel 1} = P_{1\parallel} - P_{3\parallel}$, where we introduced the designations

$$P_{1\parallel} = \sqrt{(s/4) - M^2} \quad (13)$$

and

$$P_{3\parallel} = \sqrt{\left(\frac{\sqrt{s}}{2} - E_1 \right)^2 - M^2}. \quad (14)$$

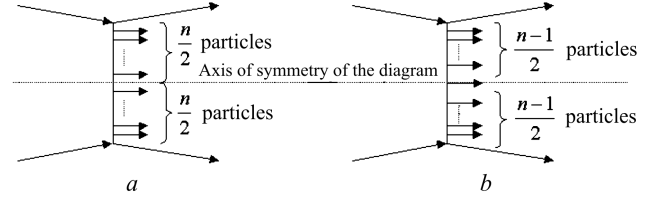


Fig. 4. Horizontal axis of symmetry of the multiperipheral diagram for the even (*a*) and odd (*b*) numbers of secondary particles

This follows from (4) with regard for all properties of the symmetry (we note that these properties yield $P_{\parallel}^s = 0$ and, therefore, $P_{3\parallel} = P_{1\parallel}$). It is worth noting the difference in the contents of $P_{1\parallel}$ and $P_{\parallel 1}$. The former stands for the component of the momentum of primary particle 1, which is parallel to the collision axis (Fig. 2). The latter denotes the parallel component of the momentum, which is transferred along virtual line 1 in Fig. 3.

In the case where the number of particles is odd, we have

$$A_0 = \prod_{j=1}^{(n+1)/2} \left(1 - (E_j)^2 + (P_{\parallel j})^2 \right)^{-2}, \quad (15)$$

where

$$E_j = (1/2) + \sum_{k=j}^{(n-1)/2} \text{ch}(y_k) \quad (16)$$

for $j = 1, 2, \dots, n-1$; $E_{(n+1)/2} = 1/2$; $P_{\parallel j}$ for $j = 1, 2, \dots, (n+1)/2$ are determined by the same relations (12), as in the case with odd number of particles. In this case, $P_{1\parallel}$ and $P_{3\parallel}$ are determined by the same relations (13) and (14), as in the case with even number of particles, but E_1 is determined by relation (16). Since all calculations are analogous for both cases of even and odd numbers of secondary particles, we will consider the case of even n in detail and present only the results for the case of odd n .

Since function (10) is a product of positive fractions, it is convenient to seek a maximum of its logarithm. We denote it by $L(n, y_1, y_2, \dots, y_{n/2})$. Then the system of equations for the determination of the stationary point of the function L can be given in the following form (we introduce the notation $Z_j = 1 - (E_j)^2 + (P_{\parallel j})^2$):

$$\frac{\partial L}{\partial y_1} = \frac{\partial L}{\partial E_1} \text{sh}(y_1) + 4\text{ch}(y_1) \sum_{j=2}^{n/2} \frac{P_{\parallel 1}(E_1) - \sum_{k=1}^{j-1} \text{sh}(y_k)}{Z_j} +$$

$$+2\text{ch}(y_1) \frac{P_{||1}(E_1) - \sum_{k=1}^{n/2} \text{sh}(y_k)}{Z_{(n/2)+1}} = 0, \tag{17}$$

$$\begin{aligned} \frac{\partial L}{\partial y_l} &= \frac{\partial L}{\partial E_1} \text{sh}(y_l) + 4\text{sh}(y_l) \sum_{j=2}^l \frac{\sum_{k=j}^{n/2} \text{ch}(y_k)}{Z_j} + \\ &+ 4\text{ch}(y_l) \sum_{j=l+1}^{n/2} \frac{P_{||1}(E_1) - \sum_{k=1}^{j-1} \text{sh}(y_k)}{Z_j} + \\ &+ 2\text{ch}(y_l) \frac{P_{||1}(E_1) - \sum_{k=1}^{n/2} \text{ch}(y_k)}{Z_{(n/2)+1}} = 0, \end{aligned} \tag{18}$$

$l = 2, 3, \dots, (n/2) - 1,$

$$\begin{aligned} \frac{\partial L}{\partial y_{n/2}} &= \frac{\partial L}{\partial E} \text{sh}(y_{n/2}) + 4\text{sh}(y_{n/2}) \sum_{j=2}^{n/2} \frac{\sum_{k=j}^{n/2} \text{ch}(y_k)}{Z_j} + \\ &+ 2\text{ch}(y_{n/2}) \frac{P_{||1}(E_1) - \sum_{k=1}^{n/2} \text{sh}(y_k)}{Z_{(n/2)+1}} = 0. \end{aligned} \tag{19}$$

In order to simplify the system of equations (17)–(19), we use the following reasoning. With regard for the negativity of virtualities $(k_j)^2$ and relation (9), it is seen that all Feynman denominators Z_j are greater than 1. In addition, all these denominators enter system (17)–(19) in the form $1/Z_j$. But the function $f(x) = 1/x$ at $x > 1$ has a small value of the derivative, i.e., the function varies slowly. This allows us to solve the system of equations (17)–(19) in the approximation, where all quantities $1/Z_j$ in this system of equations are set to be equal to one another. In addition, at the threshold value $\sqrt{s} = 2M + n$, we have $|(k_j)^2| = n(j-1) + (j-1)^2 + Mn$. If n are not small, this quantity takes large values, Therefore, for not very high energies, we have the relation $Z_j \gg 1$, which additionally favors the use of the approximation of equal $1/Z_j$. The numerical calculation indicates that this approximation can be used also at high energies, because

the virtualities become small and all Z_j are close to 1. As a result, $1/Z_j$ are again approximately equal to one another.

It was shown in [4] that, in the approximation of equal $1/Z_j$, the system of transcendental equations (17)–(19) can be solved analytically, and the solution will be given below. Let us denote the values of rapidities in the solution by $y_1^{(0)}, y_2^{(0)}, \dots, y_{n/2}^{(0)}$. Then all these rapidities can be expressed in terms of $y_{n/2}^{(0)}$ by the relation

$$y_k^{(0)} = \left(2 \left(\frac{n}{2} - k \right) + 1 \right) y_{n/2}^{(0)}, \quad k = 1, 2, \dots, n. \tag{20}$$

Using the analogous reasoning in the case of odd number of particles, we obtain [4]

$$y_k^{(0)} = \left(\frac{n-1}{2} - k + 1 \right) y_{(n-1)/2}^{(0)}, \quad k = 1, 2, \dots, n. \tag{21}$$

The quantities $y_{n/2}^{(0)}$ in (20) and $y_{(n-1)/2}^{(0)}$ in (21) can be expressed through the solution Δy of the transcendental equation

$$\frac{\sqrt{s}}{2} - \frac{\text{sh}((n/2)\Delta y)}{2\text{sh}((1/2)\Delta y)} = M \text{ch} \left(\frac{n+1}{2} \Delta y \right). \tag{22}$$

In this case, $y_{n/2}^{(0)} = \Delta y/2$, and $y_{(n-1)/2}^{(0)} = \Delta y$.

We pay attention to the fact that relations (20) and (21) involve the symmetry of the values of rapidities at the maximum point. Therefore, these formulas determine the values of rapidities not only for the vertices positioned above the symmetry axis, but for all vertices of the diagram in Fig. 3.

Near the threshold of creation of n particles, the solution of Eq. (22) takes the form

$$\Delta y = \frac{2}{n+1} \text{acosh} \left(\frac{\sqrt{s} - n}{2M} \right). \tag{23}$$

It is seen from (23) that the quantity Δy has the threshold branching point at $\sqrt{s} = 2M + n$. If we calculate the contribution of the inelastic process under consideration to the imaginary part of the elastic scattering amplitude by the Laplace method, then this threshold branching point will enter the elastic scattering amplitude thorough Δy , as is required by the unitarity. We note that if the contribution of multiperipheral diagrams to the imaginary part of the elastic scattering amplitude is calculated within the ordinary methods, i.e., without the use of the Laplace method [7, 8], then we obtain the dependence characteristic of the Regge theory, which does not contain similar branching points.

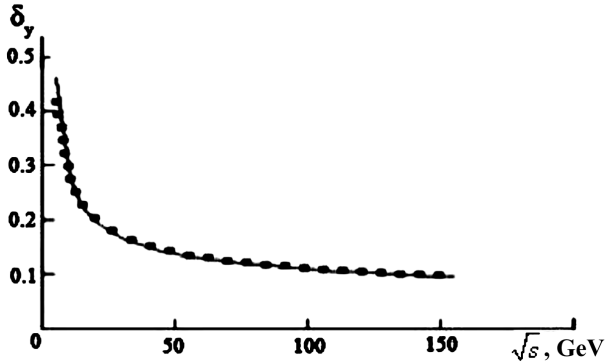


Fig. 5. Approximate solution of (25) (dashed line) and the result of numerical solution of Eq. (22) (continuous line) at $n = 10$

Prior to the determination of the quantity Δy at energies not close to the threshold one, we make several remarks. The quantity $(\text{sh}((n/2)\Delta y))/\text{sh}((1/2)\Delta y)$ in (22) has the sense of the total energy carried away by secondary particles. The quantity $2M\text{ch}(((n+1)/2)\Delta y)$ is the energy carried away by particles P_3 and P_4 . It is seen from these formulas that at high energies (and respectively Δy) the main fraction of the energy is carried away indeed by particles P_3 and P_4 . This means that the rapidity $((n+1)/2)\Delta y$ of the particle with P_3 must be slightly different from the rapidity (we denote it by Y^*) of the primary particle with P_1 . Instead of Δy , let us introduce a new variable

$$\delta_y = Y^* - (n+1)(\Delta y/2), \quad (24)$$

Its smallness allows us to solve the transcendental equation (22). We obtain the following approximate result:

$$\delta_y \approx \left(M \left(\left(\frac{\sqrt{s}}{M} \right)^{2/(n+1)} - 1 \right) \right)^{-1}. \quad (25)$$

Approximation (25) is satisfactory, which is seen from Fig. 5, where it is compared with the quite “exact” result of numerical solution of Eq. (22).

All the presented results concerning the existence of the maximum of the scattering amplitude and its properties were numerically verified in [4]. In addition, it was shown in [5] on the basis of the results of numerical calculations that the maximum is sufficiently “sharp” in order that the Laplace method can be applied.

With the help of the presented results, we can demonstrate the most significant property of the maximum point of the multiperipheral model. This property consists in that the moduli of the virtualities $|(k_l)^2|$, which are calculated at the values of variables corresponding

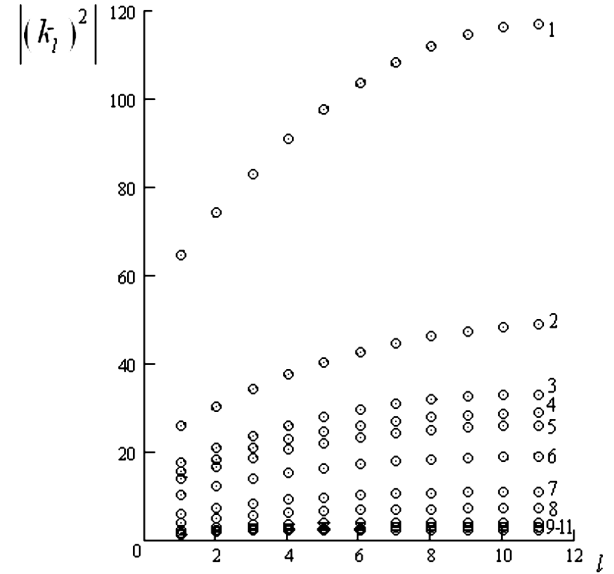


Fig. 6. Moduli of virtualities calculated at the maximum point for $n = 20$ versus \sqrt{s} . Only the virtualities of lines positioned above the symmetry axis of the diagram are shown, since the virtualities of symmetric lines are the same. Line 1 corresponds to the energy $\sqrt{s} = 5$ GeV, 2 - $\sqrt{s} = 7$ GeV, 3 - $\sqrt{s} = 9$ GeV, 4 - $\sqrt{s} = 10$ GeV, 5 - $\sqrt{s} = 11$ GeV, 6 - $\sqrt{s} = 15$ GeV, 7 - $\sqrt{s} = 30$ GeV, 8 - $\sqrt{s} = 60$ GeV, 9 - $\sqrt{s} = 200$ GeV, 10 - $\sqrt{s} = 546$ GeV, and 11 - $\sqrt{s} = 900$ GeV

to the maximum point, decrease, as the energy \sqrt{s} increases. The numerical calculation showed [4] that the moduli of the virtualities grow from a minimum value (we denote it by v_{\min}), which is attained at the first and $(n+1)$ -th lines of the diagram in Fig. 3, to the maximum value v_{\max} , which is attained on the line, which is crossed by the symmetry axis in the case with even number of particles (Fig. 4,a), or on two lines touching the axis in Fig. 4,b for an odd number of particles. The calculation of the quantities v_{\min} and v_{\max} with regard for relations (20) or (21), (24), and (25) gives the following approximate results:

$$v_{\min} = \left(\left(\frac{\sqrt{s}}{M} \right)^{2/(n+1)} - 1 \right)^{-2},$$

$$v_{\max} = \left(\left(\frac{\sqrt{s}}{M} \right)^{1/(n+1)} - \left(\frac{\sqrt{s}}{M} \right)^{-1/(n+1)} \right)^{-2}. \quad (26)$$

The drop of the moduli of virtualities with increase in the energy, which is indicated by relations (26), is confirmed by the results of numerical calculations given in Fig. 6.

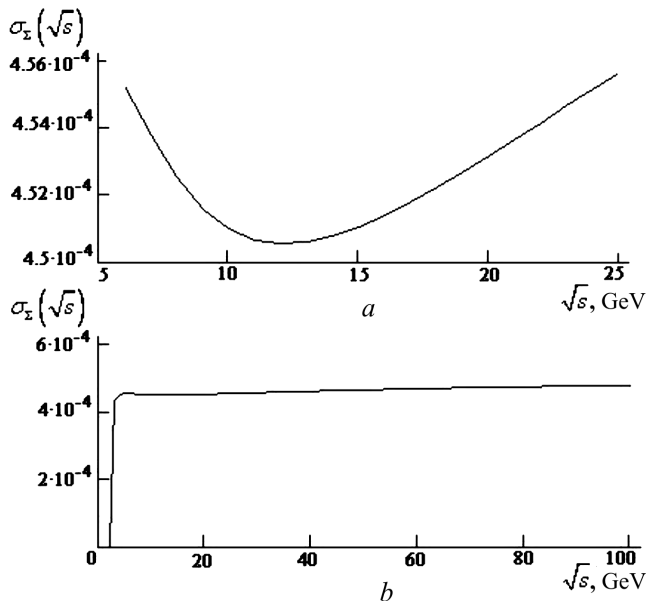


Fig. 7. Dependence of $\sigma_{\Sigma}(\sqrt{s})$, on the energy at the fitting constant $\Lambda = 5.475$ in the intervals of energies $\sqrt{s} = 7 \div 25$ GeV (a), and $\sqrt{s} = 1 \div 100$ GeV (b). The fitting constant was chosen so that the dip of the cross-section coincides approximately with that observed in the experiment on proton-proton scattering

This decrease corresponds to the new mechanism of growth of scattering cross-sections, which was not considered in the previous calculations in the multiperipheral model. Indeed, it is seen from (9) that the decrease of the moduli of virtualities causes the increase of the scattering amplitude at the maximum point, as \sqrt{s} increases. With regard for the above-presented idea of the Laplace method, we see that the square of the increasing amplitude modulus at the maximum point enters the formula for the partial scattering cross-section associated with the creation of a number of secondary particles as a factor. Then, by summing the partial cross-sections, we can obtain the total cross-section increasing with the energy with agreement with the experimental data.

However, by verifying these assertions we face the necessity of considering the interference contributions [9]. These contributions arise due to that the scattering amplitude in the frame of the multiperipheral model is represented not only by the diagram in Fig. 3, by the sum of $n!$ diagrams of such a type with all possible versions of the joining of the lines of secondary particles to the diagram. Respectively, by calculating the square of the modulus of this amplitude, we obtain a large number of “cross” (interference) terms. The integrals of them give positive contributions to the partial cross-section, which should be taken into account due to their huge number,

though the contribution of the square of the modulus of a single diagram in Fig. 3 makes a very small fraction of the resulting partial cross-section [5]. The numerical calculations show that, starting from the threshold of creation of n particles, there exists a quite wide interval of energies, at which the eigenvalues of the matrix of secondary derivatives of the logarithm of the scattering amplitude with respect to the rapidities can be considered close to one another. At such energies, the approximate method to determine the interference contributions to partial cross-sections was proposed in [9].

If the partial cross-sections are calculated, we can consider the quantity

$$\sigma_{\Sigma}(\sqrt{s}) = \sum_{n=1}^{n_{\max}} \Lambda^n \sigma'_n(\sqrt{s}), \tag{27}$$

where $\sigma'_n(\sqrt{s})$ is defined in relation (8), and we introduced the notation

$$\Lambda = \frac{\lambda^2}{2(2\pi)^3} \tag{28}$$

for the dimensionless coupling constant, which is considered as a fitting parameter. In addition, by n_{\max} , we denoted the maximum number of secondary particles, whose creation is allowed by the energy conservation law. The quantity $\sigma_{\Sigma}(\sqrt{s})$ is an analog of the total scattering cross-section in the model under consideration. As is seen from Fig. 7, we can take the fitting constant Λ such that the dependence of that quantity on the energy \sqrt{s} will be analogous to the one observed in experiment for the total hadron-hadron scattering cross-section (Fig. 7). Unfortunately, we attain only the qualitative description of experimental data. To obtain the quantitative agreement, it is necessary to develop a model more realistic than the model of interaction of two real scalar fields.

Nevertheless, we may conclude that the mechanism of the virtualities reduction, which is peculiar to more realistic models as well, indeed can claim to be the mechanism responsible for the increase of the total cross-section with energy, which is observed in experiments.

The question arises whether this growth agrees with the Froissart bound [10]. As is seen from relations (26) and Fig. 6, the mechanism of decrease of the virtualities with increase in the energy “is switched-off”. Relations (26) imply that this occurs under the condition

$$\sqrt{s} \gg M \exp((n + 1) \operatorname{asinh}(1/2)). \tag{29}$$

In this case, the formula of a partial cross-section contains the factor [5, 9]

$$\left(\sqrt{s}\sqrt{\frac{s}{4}-M^2}\left(\frac{E_P}{2}\right)\sqrt{\left(\frac{E_P}{2}\right)^2-M^2}\right)^{-1}$$
 (where E_P is determined by relation (4) at zero transverse momenta and rapidities (20) or (21)). At high energies, this factor behaves itself as s^{-2} . Its denominator contains, according to (29) at the maximum point of $\sigma'_n(\sqrt{s})$ at a certain n , the quantity $\approx \exp(4(n+1)\operatorname{asinh}(1/2))$. Thus, if the fitting constant satisfies approximately the condition

$$\ln(\Lambda) < 4\operatorname{asinh}(1/2), \quad (30)$$

the values of $\Lambda^n \sigma'_n(\sqrt{s})$ at the points of their maxima will decrease, as n increases. At sufficiently high energies, the terms with large n will give a small contribution to sum (27), and the terms with small n will decrease due to the “switching-off” of the mechanism of decrease of the virtualities. In such a case, the total cross-section (27) must have the asymptotics, which decreases, as the energy increases.

To confirm the above reasoning, we mention the results presented in Fig. 8. On their basis, we may conclude that the growth of the total cross-section due to a decrease of virtualities can be consistent with the Froissart bound

Thus, within the multiperipheral model with the help of the Laplace method, we have obtained the results, which differ significantly from those obtained within the same model by different methods [6–8]. Therefore, it is natural to analyze the reasons for such a difference. The main reason consists in that the approximations made in the calculation of the multidimensional integral (1) did not consider the dependence of the integrand on the components of the momenta of secondary particles in the center-of-mass system, which are longitudinal relative to the collision axis. But, as we have seen, this dependence is essential, because it is not reduced to a constant and has a maximum. In addition, the increase of the value of this maximum with the energy \sqrt{s} is a result of the dependence of the scattering amplitude on rapidities, which cannot be revealed, of course, if this dependence is neglected.

Let us consider some other types of diagrams, where the Laplace method can be used.

4. Some Types of Diagrams Admitting the Application of the Laplace Method

Consider a diagram of the type shown in Fig. 9,a and, in particular, a separate block of this diagram (Fig. 9,b).

Below, we consider some examples of various blocks (Fig. 9,b), which correspond to the analytic formu-

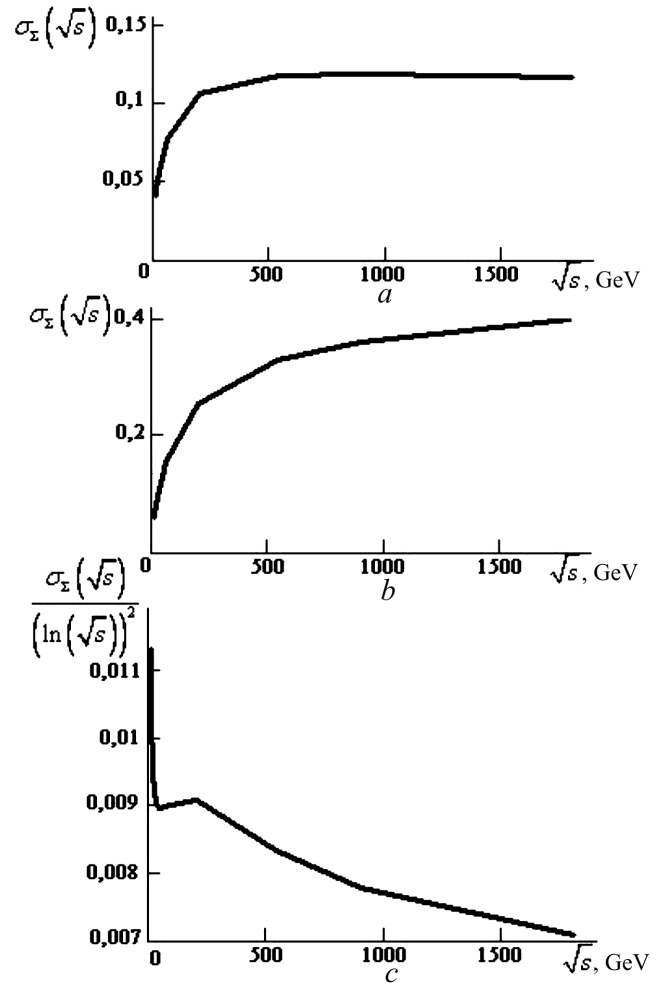


Fig. 8. Calculated values of (27) in the interval of energies $\sqrt{s} = 10 \div 1800$ GeV with regard for the interference contributions within the method in [9] for various values of the fitting constant $\Lambda = \exp(3.9\operatorname{asinh}(\frac{1}{2}))$ (a), $\Lambda = \exp(4.1\operatorname{asinh}(\frac{1}{2}))$ (b,c) and the ratio $\sigma_\Sigma(\sqrt{s})/(\ln(s))^2$, whose decrease with increase in the energy \sqrt{s} (c) supports the validity of the Froissart bound.

las that possess the following property. The maximum value of the modulus of the corresponding expression is attained not at certain values of the four-momenta $p_{i_1}, p_{i_2}, \dots, p_{i_b}$, but only if all these four-momenta are equal to one another. At the same time, these four-momenta enter the expression corresponding to the remaining part of the diagram only in the form $\sum_{j=1}^b p_{i_j}$. Therefore, the condition of maximum for this expression will fix only the value of this sum. Thus, the same values of the four-momenta $p_{i_1}, p_{i_2}, \dots, p_{i_b}$ can satisfy the conditions of maximum for this block and for the rest of the diagram.

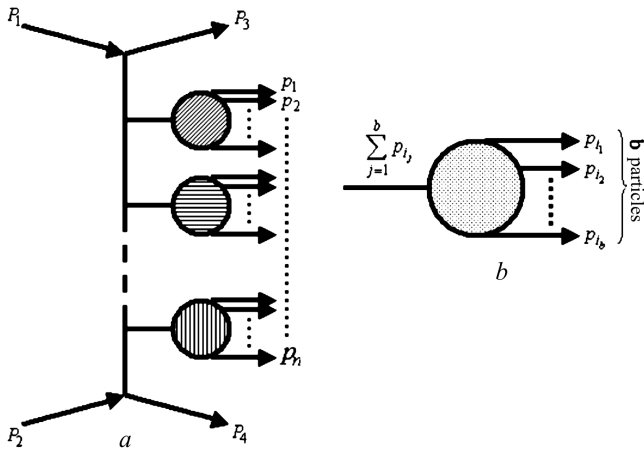


Fig. 9. Diagram of the inelastic scattering with arbitrary blocks, where secondary particles are created (a), and its separate block (b). The dashed block means an arbitrary diagram with the appropriate number of external lines. Blocks can be identical or different from one another, which is marked by different hatches

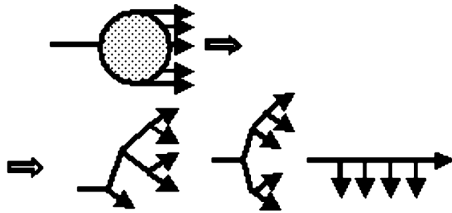


Fig. 10. Versions of blocks without loops with 5 particles joining a block

The simplest examples of blocks, for which the condition of maximum is the equality of all four-momenta of secondary particles, which join the block, are the blocks of diagrams without loops. For example, we can consider three versions of such diagrams for a loopless block with 5 particles joining it (Fig. 10).

Each internal line of a loopless block corresponds to a factor of the type $1/(1 - (\sum p_i)^2 - i\varepsilon)$, where the number of terms in the sum $\sum p_i$ is not less than 2. Therefore, these factors give no poles in the integration region, and the parameter ε can be turned to zero else before the subsequent calculations (in this case, $|1/(1 - (\sum p_i)^2)| = 1/((\sum p_i)^2 - 1)$). As is seen, each such factor attains the maximum value under the condition of minimum for the quantity $(\sum p_i)^2$, which has sense of the square of the summary energy of those particles, whose four-momenta enter the sum, in the system of their center of masses. But this energy will be minimal, if all momenta of particles in the center-of-mass system are zero. Thus, the minimal value of the Lorentz-

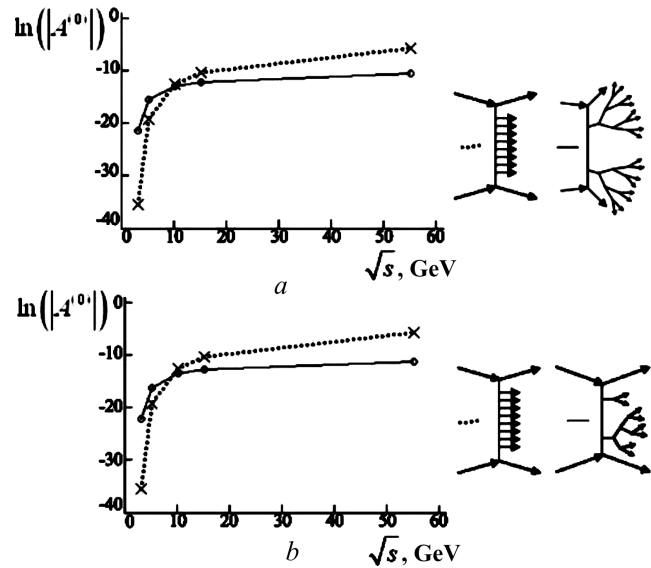


Fig. 11. Dependence of the logarithm of the modulus of the scattering amplitude on \sqrt{s} at the maximum point $|A^{(0)}|$ for various types of diagrams

invariant $(\sum p_i)^2$ is attained at identical values of all four-momenta, which enter the sum.

We note that, in the scalar theory considered here, each block corresponds to some scalar function of the four-momenta of secondary particles joining the block. Due to the proved property, this function can be replaced in the search for the maximum of the modulus of the scattering amplitude that corresponds to the whole diagram by its restriction, where all four-momenta are equal to the same value p . But the scalar function of a single four-vector p can be only a function of $p^2 = 1$, i.e., it is a constant. Therefore, after the transition to the mentioned restriction, the further maximization is performed analogously to the above-considered case of the multiperipheral diagram in Fig. 3.

We denote that the diagrams with loopless blocks, like the multiperipheral diagrams in Fig.3, have the constrained maximum point, and both types of diagrams with the same number of secondary particles have the same order in the coupling constant. These facts allow us to compare the moduli of the appropriate amplitudes at the maximum point (Fig. 11). As is seen, there exists a sufficiently wide interval of energies \sqrt{s} near the threshold of creation of a certain number of secondary particles, where the contribution of the diagrams with loopless blocks will be more significant than the contribution of simple multiperipheral diagrams. Since, at any energy, there exist such multiplicities n of secondary particles, for which we will be sufficiently close to the

threshold, we can conclude about the necessity to take the diagrams with loopless blocks into account.

In the above-considered diagrams, all Feynman denominators are more than 1 in modulus. Therefore, as is seen from the above-presented results, the values of the dimensionless scattering amplitude at the maximum points are small. This induce the desire to consider the diagrams with loops, in which the terms corresponding to lines have poles. Such integrable singularities can lead to larger values of the scattering amplitude. With the purpose to obtain such diagrams, let us consider the system of three interacting scalar fields with the Lagrangian

$$\tilde{L} = \frac{1}{2} (g^{ab} \Phi_{,a} \Phi_{,b} - M^2 \Phi^2) + \frac{1}{2} (g^{ab} \varphi_{,a} \varphi_{,b} - m^2 \varphi^2) + \frac{1}{2} g^{ab} \chi_{,a} \chi_{,b} + g \Phi^2 \chi + \lambda \chi^2 \varphi + \lambda_1 \chi^3 + \lambda_2 \chi^4, \quad (31)$$

where λ_1 and λ_2 are the corresponding coupling constants made dimensionless with mass m . In other words, the fields Φ and φ , which have the same meaning as above, interact with each other not directly, but through a scalar massless field χ considered as a scalar analog of gluons. In the theory with Lagrangian (31), there appear diagrams of the type of those shown in Fig. 12.

We note that if one secondary particle is created on some loop (see Fig. 12), the integral over such a loop contains the singularity, which can be removed by renormalizing the constant λ in Lagrangian (31). Then the finite part of the integral corresponding to the loop can be sufficiently easily calculated. Therefore, we will consider the loops, where the number of created particles is at least two. We will prove that the modulus of an analytic expression corresponding to each loop on the diagram in Fig. 12 attains the maximum value under the condition of equal four-momenta of all secondary particles joining the loop.

One loop in Fig. 12 is described by the following analytic expression:

$$A = (-1)^{b+1} \int d^4 q (q^2 + i\varepsilon)^{-1} \times \prod_{j=1}^b \left(\left(q - \sum_{k=1}^j p_k \right)^2 + i\varepsilon \right)^{-1}. \quad (32)$$

Here, the number of particles joining the loop is denoted by b , and their four-momenta are enumerated, for convenience, irrespective of other four-momenta of particles on the diagram (i.e., p_1, p_2, \dots, p_b).

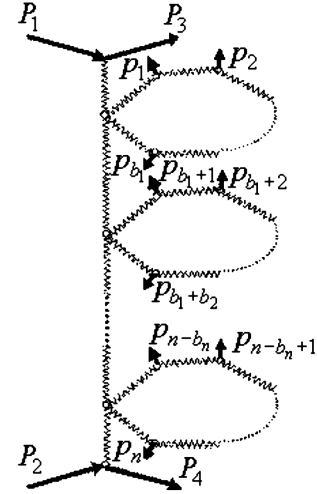


Fig. 12. Diagram with loops. Wavy lines correspond to the field χ . The number of loops is denoted by l , and the numbers of secondary particles joining each loop are b_1, b_2, \dots, b_l , respectively

By applying the Feynman identity [11] to integral (32), we can write it as

$$A = i (-1)^{b-1} (b-2)! \pi^2 \times \int_0^1 dz_1 \int_0^{z_1} dz_2 \dots \int_0^{z_{b-1}} dz_b \frac{1}{(d + i\varepsilon)^{b-1}}, \quad (33)$$

where we introduced the notation

$$d = \sum_{i=1}^b z_i (1 - z_i) + 2 \sum_{i=1}^{b-1} \sum_{j=i+1}^b z_j (1 - z_i) (p_i p_j). \quad (34)$$

The integration region in (33) is such that all quantities $z_j (1 - z_i)$ are nonnegative. Therefore, the minimum of the modulus of the denominator d is attained at minimally possible values of all scalar products $(p_i p_j)$. This is realized under the condition that all these four-momenta are equal to one another. Thus, in the further maximization of the modulus of the expression corresponding to the diagram in Fig. 12, the expression describing each loop can be replaced by its restriction on the set of identical four-momenta. The calculation of integral (32) at arbitrary four-momenta of secondary particles would be very complicated task. However, under the mentioned restriction, the problem is simplified so that the integral can be calculated analytically. Denoting, by A_0 , the value of integral (32) for equal four-momenta $p_1 = p_2 = \dots = p_b$, we obtain

$$A_0 = \pi^3 \left(\frac{(-1)}{(b-2)! (b-2)! b} + (-1)^{b-1} I_1(b, j) + \right.$$

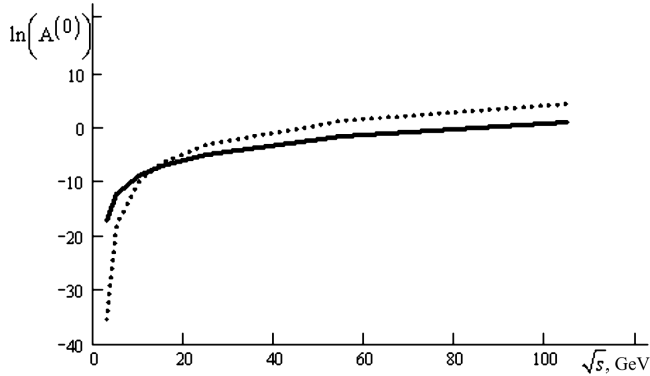


Fig. 13. Logarithms of the moduli of the values of the scattering amplitude at the maximum points for the one-loop diagrams in Fig. 12 (continuous line) and in Fig. 3 (dashed line) for $n = 8$

$$\begin{aligned}
 & + \sum_{f=2}^{b-2} (-1)^{b-f} I_2(b, j, f), \\
 I_1(b, j) & = \frac{1}{(b-1)!b!} + \\
 & + \sum_{j=2}^{b-1} \frac{1}{j!(b-j)!(b-j+1)!(j-1)!}, \\
 I_2(b, j, f) & = f \left(\frac{1}{(b-f)!b!(f-1)!} + \right. \\
 & \left. + \sum_{j=f+1}^{b-1} \frac{1}{j!(b-j)!(f+b-j)!(j-f)!} \right). \tag{35}
 \end{aligned}$$

The theory with Lagrangian (31) contains also multiperipheral diagrams of the type shown in Fig. 3, but with the replacement of vertical lines by wavy lines of the field χ . These diagrams and the diagrams in Fig. 12 have different orders in the coupling constant. However, a diagram of the type shown in Fig. 12 with one loop contains only a single “superfluous” vertex, as compared with the diagram in Fig. 3 with the same number of particles. We will try to compare the logarithms of the moduli of the scattering amplitudes corresponding to these diagrams. Taking into account that, for any “reasonable” value of the coupling constant, its logarithm is of the order of several units, we give, however, the appropriate comparison for the case of diagrams, where 8 secondary particles are created, in Fig. 13.

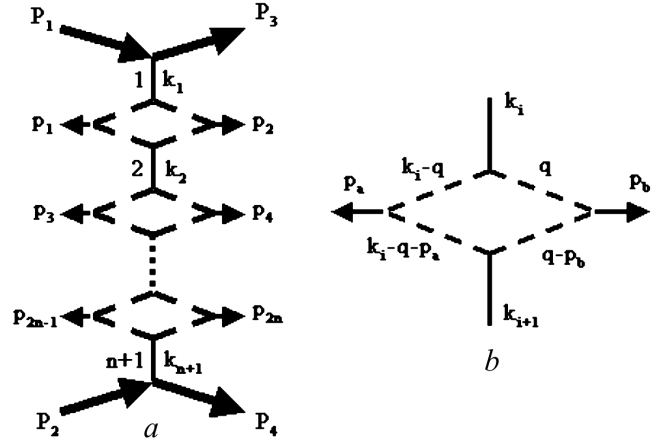


Fig. 14. Diagram with “four-corner” vertices (a) instead of simple vertices in Fig. 3 and its four-vertex block (b)

It is seen from the results presented in Fig. 13 that, at low energies, the domination of the contribution of the one-loop diagrams is so significant that it cannot be influenced by any “reasonable” value of the coupling constant.

Thus, the application of the Laplace method allows one, on the one hand, to extend the circle of the diagrams of the inelastic scattering admissible for calculations and, on the other hand, indicates the necessity to consider, in addition to multiperipheral diagrams, diagrams of other types.

Let us consider a simple scalar analog of the formation of hadrons from quarks in a model with the Lagrangian

$$\begin{aligned}
 \tilde{L} & = \frac{1}{2} (g^{ab} \Phi_{,a} \Phi_{,b} - M^2 \Phi^2) + \frac{1}{2} (g^{ab} \varphi_{,a} \varphi_{,b} - m^2 \varphi^2) + \\
 & + \frac{1}{2} (g^{ab} \xi_{,a} \xi_{,b} - m_q^2 \xi^2) + g \Phi^2 \varphi + \lambda \xi^2 \varphi, \tag{36}
 \end{aligned}$$

where, by m_q , we denoted a mass of 0.338 GeV made dimensionless with the pion mass m . Such a mass is approximately equal to the mean mass of light quarks. The model with Lagrangian (36) contains the diagrams shown in Fig. 14,a (dashed lines correspond to the field ξ).

The main problem of maximization of the modulus of the scattering amplitude corresponding to the diagram in Fig. 14,a consists in the calculation of the integral for the four-vertex loop in Fig. 14,b. The symmetry of the diagram implies that if the modulus of the scattering amplitude has the maximum point, then this maximum should be attained at equal four-momenta $p_a = p_b = p$ of the particles joining each four-vertex loop. Therefore,

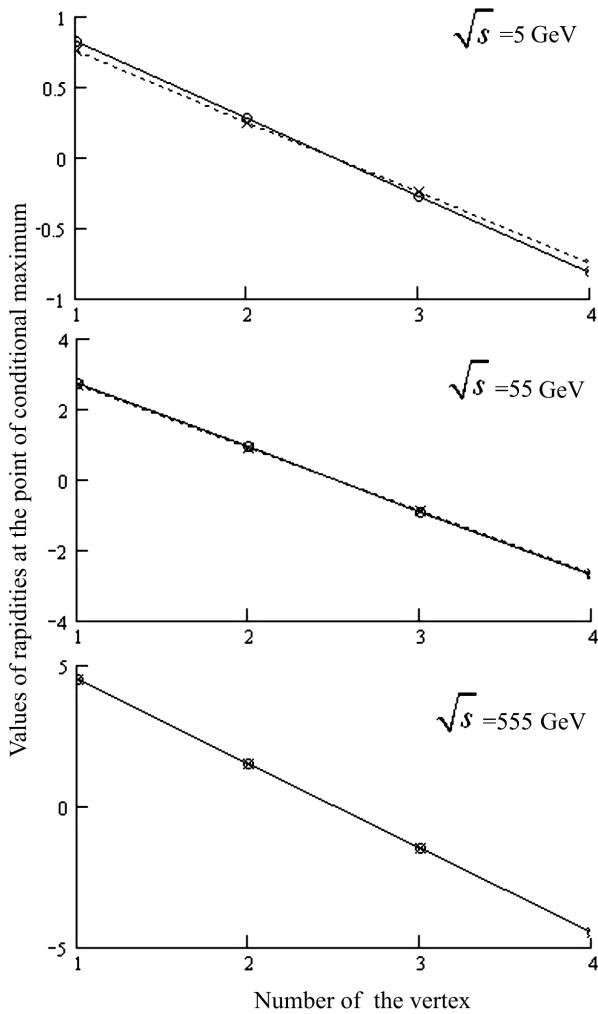


Fig. 15. Values of rapidities at the point of constrained maximum of the modulus of the scattering amplitude for the diagram in Fig. 12,*a* with simple and “four-corner” vertices. For convenience, the points are connected by lines: dashed lines for simple vertices and continuous lines for “four-corner” vertices

by setting these momenta to be identical, we can further maximize the obtained restriction of the scattering amplitude. This simplifies significantly the calculation of the integral corresponding to the loop in Fig. 14,*b*. After this simplification, the integral over the four-vertex loop can be transformed into a single integral. The final expression of this integral is awkward and is omitted here. But it turns out to be quite suitable for the subsequent numerical maximization of the moduli of the scattering amplitudes corresponding to diagrams of the type shown in Fig. 14,*a* with a small number of four-vertex loops.

The values of rapidities at the maximum point for a diagram with 4 “four-corner” vertices are given in Fig.

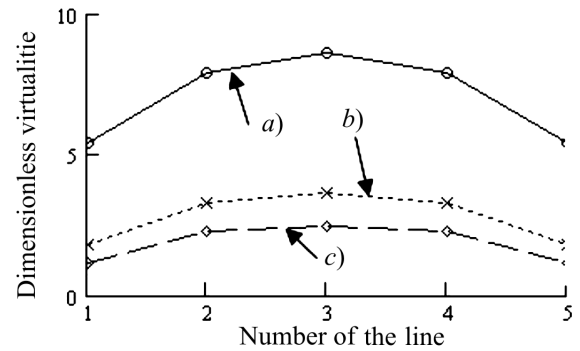


Fig. 16. Dependence of the dimensionless virtualities at the maximum point for vertical lines of the diagram in Fig. 14,*a* with four “four-corner” vertices on the energy. Line *a*) corresponds to the energy $\sqrt{s} = 5$ GeV, *b*) $\sqrt{s} = 10$ GeV, *c*) $\sqrt{s} = 15$ GeV

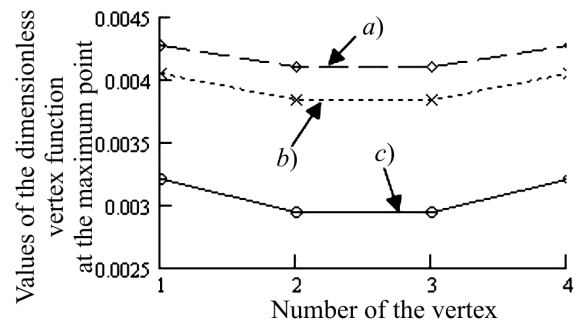


Fig. 17. Increase of the modulus of the function corresponding to the “four-corner” vertex in Fig. 14,*b* with the energy. Line *a*) corresponds to the energy $\sqrt{s} = 15$ GeV, *b*) $\sqrt{s} = 10$ GeV, *c*) $\sqrt{s} = 5$ GeV. The enumeration of vertices corresponds to Fig. 14,*a*: the first vertex is that, into which the first vertical line in the diagram in Fig. 14,*a* enters, etc.

15. The comparison with the maximization of an analogous diagram with simple vertices indicates that the replacement of the constant corresponding to a simple vertex by the complicated expression corresponding to the “four-corner” vertex diagram in Fig. 14,*b* changes slightly the result of the maximization. In this case, the difference between these results becomes insignificant, as the energy increases.

In Fig. 16, we show the results of calculations of the values of virtualities at the maximum point, which correspond to vertical lines of the diagram (the enumeration of lines is shown in Fig. 14,*a*) at various energies. It is seen from Fig. 16 that the basic mechanism of growth of cross-sections, which is related to a decrease of the virtualities, is conserved for the diagrams with “four-corner” vertices.

In addition, we indicate the new mechanism of growth, which is caused by the increase of the moduli of the

relevant functions with the energy at the maximum point corresponding to “four-corner” vertices (Fig. 17).

Thus, the results of this section allow us to conclude that there exist the quite many types of diagrams, which can be calculated by the Laplace method. In this case, the fact that we don't have to know the values of complicated integrals for all values of external momenta, but only in a small neighborhood of the maximum point, simplifies significantly the consideration of these integrals and enables to treat new diagrams earlier inaccessible for calculations.

1. A.B. Kaidalov, Usp. Fiz. Nauk **173**, 1153 (2003).
2. V.A. Abramovskii, V.N. Gribov, and O.V. Kancheli, Yad. Fiz. **18**, 595 (1973).
3. N.G. de Bruijn, *Asymptotic Methods in Analysis* (Interscience, New York, 1958).
4. I.V. Sharf, G.O. Sokhrannyi, A.V. Tykhonov, K.V. Yatkin, N.A. Podolyan, M.A. Deliyergiyev, V.D. Rusov, hep-ph/0605110 (2006).
5. I.V. Sharf, G.O. Sokhrannyi, A.V. Tykhonov, K.V. Yatkin, N.A. Podolyan, M.A. Deliyergiyev, V.D. Rusov, arXiv: 0711.3690 (2007).
6. D. Amati, A. Stanghellini, and S. Fubini, Nuovo Cimento **26**, 896 (1962).
7. I.G. Halliday and L.M. Saunders, Nuovo Cimento A **60**, 115 (1969).

8. Yu.P. Nikitin and I.L. Rosental', *High-Energy Nuclear Physics* (Atomizdat, Moscow, 1980) (in Russian).
9. I.V. Sharf, A.V. Tykhonov, G.O. Sokhrannyi, K.V. Yatkin, and V.D. Rusov, arXiv: 0912.2598 (2009).
10. M. Froissart, Phys. Rev. **123**, 1053 (1961).
11. P. Ramon, *Field Theory* (Pergamon, New York, 1982).

Received 16.03.11.

Translated from Ukrainian by V.V. Kukhtin

МЕТОД ЛАПЛАСА ДЛЯ ОПИСУ НЕПРУЖНОГО РОЗСІЯННЯ АДРОНІВ І НОВІ МЕХАНІЗМИ ЗРОСТАННЯ ПЕРЕРІЗІВ

I.V. Шарф, А.В. Тихонов, Г.О. Сохранний, К.В. Яткін, М.А. Делиєргієв, Н.О. Подольні, В.Д. Русов

Резюме

Показано, що існують типи фейнманівських діаграм, для розрахунку яких можна застосувати метод Лапласа, що дозволяє виявити нові механізми зростання перерізів розсіяння, які не враховуються реджіонною теорією внаслідок нехтування залежністю амплітуди розсіяння від поздовжніх компонент імпульсів вторинних частинок у системі центра мас вихідних частинок. У межах мультипериферичної моделі отримано залежність повного перерізу розсіяння від енергії, яка на якісному рівні збігається з експериментальною залежністю.